

COMETARY PLASMAS AND THE SOLAR WIND

A Thesis
Presented to
the Faculty of the Department of Physics
University of Houston

In Partial Fulfillment
of the Requirements for the Degree
Master of Science

by
Michael E. Shelby
August 1968

450499

ACKNOWLEDGEMENTS

I would like to thank Doctor John Kern for suggesting the problem and for the many enlightening discussions over the physics involved in it. I would like to thank my advisor Doctor Natalie Kovar for her patient reading and re-reading of the manuscript. Finally, I would like to thank Mr. Howard Schmidt and Mr. Neil Sams for help with the computer programming.

COMETARY PLASMAS AND THE SOLAR WIND

An Abstract of a Thesis

Presented to

the Faculty of the Department of Physics

University of Houston

In Partial Fulfillment

of the Requirements for the Degree

Master of Science

by

Michael E. Shelby

August 1968

ABSTRACT

The interaction between a comet and the solar wind has been treated extensively in the literature. Solution of the general flow problem, for example, has been considered by Ioffe (1966), Kovar and Kern (1966), and Biermann, Brosowski, and Schmidt (1967) among others. The general approach in these treatments has been that of gas dynamics. Both a shock front (on the sunward side of the comet) and a contact discontinuity are thought to form.

In the present treatment, for the region interior to the contact discontinuity, an alternate approach is taken. Namely, the assumption is made that the ions moving away from the comet's nucleus are non-interacting and that these ions are specularly reflected back into the region bounded by the contact discontinuity by the solar wind's frozen-in magnetic field. A model is developed which predicts the size and shape of the contact discontinuity and the density of plasma interior to it. Results of this model agree well with observational data.

TABLE OF CONTENTS

Chapter	Page
I Introduction.....	1
II General Characteristics of Comets.....	3
A. General Introduction.....	3
B. The Nucleus.....	3
C. The Coma.....	4
D. The Tail.....	10
III The Proposed Model.....	12
A. Introduction.....	12
B. Discussion of the Proposed Model.....	12
IV The Contact Discontinuity.....	17
A. The Pressure Equation.....	17
B. Calculated Shape of the Cavity.....	18
C. Calculated Size of the Cavity.....	21
V The Ion Density in the Coma and Tail.....	27
A. The General Problem.....	27
B. The Density Contribution from First Order Reflections.....	27
C. The Total Density.....	30
D. The Caustics.....	31
E. The Effects of Higher Order Reflections.....	34

Chapter	Page
VI Application of Model to Actual Comets.....	41
A. Shape of the Contact Discontinuity.....	41
B. The Contours of Constant Density.....	42
C. Time Dependent Phenomena.....	48
VII Summary and Conclusions.....	51

TABLE OF FIGURES

Figure	Page
1. Spectral Trace of Comet Ikeya (1964f).....	5
2. Orientation of the Shock and Contact Discontinuity around a comet.....	13
3. Geometry of Pressure Balance.....	17
4. The Contact Discontinuities (limiting cases).....	20
5. The Contact Discontinuities (intermediate cases).....	22
6. On-axis Stopping Distance as a Function of Production Rate of Neutrals.....	23
7. On-axis Stopping Distance in the Critical Range of β	25
8. Ratio of Cross Section of Cavity at Infinity to On-axis Stopping Distance.....	26
9. Geometry of the Reflection Process.....	28
10. The Ion Trajectories.....	32
11. The Caustics.....	35
12. Flaring of the Contact Discontinuity.....	38
13. Comparison of the Cavity Outline with Observational Data.....	43
14. Density Contours for the Case of Small Mass Production Rate.....	44
15. Density Contours for the Case of Large Mass Production Rate.....	45
16. Density Contours Associated with the Surface $R = \sec(\theta/2)$	46
17. Evolution of a Ray.....	50

CHAPTER I

INTRODUCTION

A general introduction to cometary physics is contained in Chapter II. Emphasis is placed upon recent work in this field relevant to the present thesis and upon pertinent observational data. The possible ionization mechanisms, for example, photoionization, charge exchange, and "cascade ionization", of neutral molecules ejected from the comet's are discussed in detail. Anomalies in the plasma density in the coma and tail are pointed out.

Chapter III presents the model investigated. The two major assumptions are discussed in detail. These are: (1) There is no magnetic field interior to the interface separating cometary material from the solar wind. (2) The ions moving away from the comet's nucleus are specularly reflected from this interface. An analytic expression for the density of the outflowing ions is also obtained in this chapter.

The size and shape of the contact discontinuity are found in Chapter IV. The solutions are in terms of familiar functions for two limiting cases, but in the general case (due to the non-linear nature of the differential equation involved) solutions were obtained numerically. The parameters determining the scaling of the cavity are discussed and appropriate values are adopted for them.

Chapter V contains the formal solution for the density contours inside the contact discontinuity. A unique feature of the ion density in this region is a discontinuous jump across a boundary termed the

caustic. This curve is investigated in detail. Higher order reflections are also investigated in this chapter and are found to be insignificant.

Correlations between the model and observational data are noted in Chapter VI. It is found that the predicted ion density and the size and shape of the cavity agree well with observational data. Furthermore, the model predicts the existence of structure in a comet's tail which, again, agrees with observational data. Other correlations, especially those of a time dependent nature, are suggested by the model but are not considered to be conclusive.

Chapter VII summarizes and concludes the thesis.

CHAPTER II

GENERAL CHARACTERISTICS OF COMETS

A. General Introduction

A comet may be divided into three characteristic parts: a solid central body - the nucleus, an atmosphere consisting of gas and dust surrounding this nucleus - the coma, and a bounded region of gas and/or dust extending away from this nucleus - the tail. When first photographically detected, a comet is indistinguishable from an asteroid. As the comet approaches the sun, however, it begins to develop an atmosphere. The generation of this atmosphere is a consequence of the heating of the nucleus by solar radiation. In this manner, molecules are sublimated and possibly desorbed from the comet's nucleus. In addition, considerable dust is also liberated in this process. Resonant scattering of solar photons from the gas molecules and non-resonant scattering (reflection) from the dust particles in the coma and tail make comets visible when they are within 1.5 a. u. of the sun.

B. The Nucleus

The radiation scattered from the coma particles generally obscures the comet's nucleus; only rarely can a definite outline of the nucleus be seen. Hence, its mass, size, and structure must be determined indirectly. Observations of planetary perturbations of comet orbits place the mass of a typical comet at 10^{19} grams (10^{-9} times the mass of the Earth). The total mass, along with an estimated density of about 5 gm/cm^3 , determine an approximate

radius of the nucleus - about one to ten kilometers.

For some time it was thought that the nucleus was not a single body, but rather a localized cluster of particles. A rather detailed account of this "sand-bank" model is given, for example, in Beer, Lyttleton, and Richter (1963). Whipple (1955) has presented convincing arguments against such a structure for the nucleus and has introduced new arguments for a single nucleus. He envisions the nucleus as a solid, icy-like structure in which considerable dust is embedded.

C. The Coma

Surrounding the nucleus and extending out to about 10^4 - 10^6 kilometers is the comet's coma. It is approximately spherical in shape and usually exhibits little inhomogeneity. Occasionally, however, on the sunward side of the coma, concentric light and dark spaces called halos or envelopes appear. These circular regions may either remain stationary or expand outward at a typical rate of 1 km/sec (Wurm, 1963). Another type of density irregularity manifests itself through the phenomenon termed an outburst, which may be described as a sudden general increase in the brightness of the coma. Most noted for these outbursts is Comet Schwassmann-Wachmann (1925 II). On several occasions this comet has been observed to increase in brightness by as much as six magnitudes* in a period of several hours. Outbursts having $\Delta m=1$ or $\Delta m=2$ have been observed in several other comets. At present, the cause of outbursts is not certain. However, the expulsion of a large quantity of material from the

*Changes in magnitude, m , are related to changes in light intensity, I , by the equation $m_2 - m_1 = 2.5 \log(I_1/I_2)$.

comet's nucleus, with a resulting increase in scattered solar radiation, could account for this phenomenon. According to Whipple's "icy-conglomerate" model, the sudden expulsion of matter could be due to a pressure differential caused by liberation and heating of gas in localized pockets within the comet's nucleus.

A spherical, steady-state coma consisting of molecules, free radicals, and dust particles is generally observed. Almost all comets have atmospheres rich in C_2 and CN. It is these molecules that determine the visual extent of most comet atmospheres. In Figure 1 is reproduced a photoelectric spectral tracing (obtained with the Mount Wilson 60 inch reflector) of Comet 1964f (Ikeya) (Kovar and Kovar, 1965) illustrating the prominent CN, C_2 bands. Cometary comas

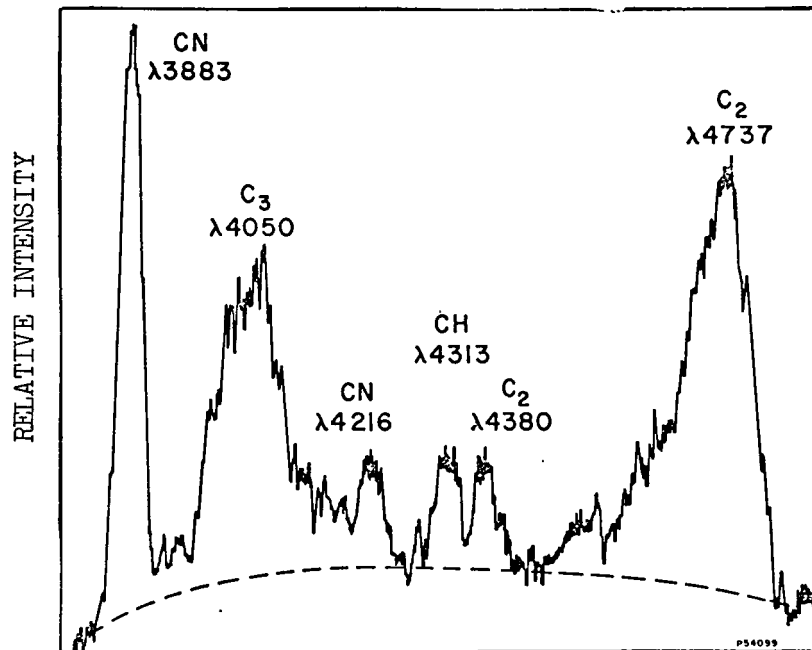


Figure 1

have also been observed to contain C_3 , CH, OH, and NH_2 in varying degrees. In general, the observed molecules are thought to be daughter molecules having their origin in larger molecules initially sublimated from the comet's nucleus. Suggested parent molecules include CH_4 , C_2H_2 , $(CH_2)_2$, C_3H_4 , H_2O_2 , C_3H_6 , NH_3 , and H_2O (Cheredichenko, 1959). It has been proposed that hydrated forms of these molecules, such as $CH_4 \cdot 6H_2O$, may constitute the nucleus (Whipple, 1963).

As comets approach within about 0.5 a. u. of the sun, atomic emissions are seen. Notably, the Sodium D doublet, the forbidden lines at $\lambda\lambda 5577$, 6300, and 6363 Å of atomic oxygen, and lines from nickel and iron have been isolated (Swings, 1965). Lines from neutral potassium, chromium, magnesium, and copper and from ionized calcium were recently found in Comet Ikeya-Seki (1965f) (Preston, 1967). The presence of the forbidden oxygen lines presents a difficulty. Wurm (1963) has noted that these lines cannot be due to resonant excitation by solar photons. The abundance of oxygen is many orders of magnitude too small. Collisional excitation by electrons is also inadequate (Remy-Battiau, 1962). By considering a combination of molecular and atomic processes, Kovar and Kovar (1966) have obtained good agreement with the observed ratio of line intensities. Warner's recent observation of an anomalous ratio of line strengths of the Sodium D doublet in Comet 1962 III is yet another anomaly in atomic cometary spectra. Once again, the usual resonance excitation mechanism fails to provide an explanation for the phenomenon. Optical pumping has been invoked as an explanation for the anomalous population of the spin states in sodium (Kovar and Kovar, 1968).

It should be pointed out that several lines appearing in the spectra of comets are as yet unidentified. Laboratory identification of molecular spectra is not complete enough to identify these unknown lines. Also to be noted is that many molecules may be present whose bands are as yet unobserved. In some cases this can be attributed to the low abundance of the molecule or weak oscillator strength of the transitions. In other cases, a molecule may remain unidentified because its bands and those of a more abundant molecule or a telluric feature overlap.

In addition to the neutral constituents of the coma, ionized molecules are also present. The relative abundances of neutral molecules and ions varies from comet to comet. The identified ions include CO^+ , N_2^+ , CO_2^+ , CH^+ , and OH^+ . Comparing these ions with the observed neutral molecules, it is apparent that, with the exception of the pairs $\text{CH}-\text{CH}^+$ and $\text{OH}-\text{OH}^+$, either the neutral or the ionized form of a given molecule has been observed but not both. It would be of considerable interest to know the ratio of ions to neutrals for the various components of the coma. The pairs $\text{CH}-\text{CH}^+$ and $\text{OH}-\text{OH}^+$ are too weakly present to provide reliable ratios of this type. In the remaining more abundant pairs, $\text{CO}-\text{CO}^+$, $\text{CO}_2-\text{CO}_2^+$, N_2-N_2^+ , $\text{CN}-\text{CN}^+$, and C_2-C_2^+ , only one member of each pair has been observed (Swings, 1965). In these cases, the undetected member has its resonant electronic transitions in the unobservable ultraviolet.

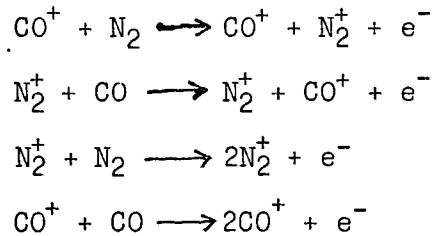
It should be noted that ionization can be brought about by more than one mechanism and that the effectiveness of a given mechanism will differ for the different pairs. Photoionization by solar radiation

is undoubtedly a significant ionization process. However, Biermann (1953) postulated that charge exchange between a stream of ionized solar particles and cometary neutrals might also be an effective ionization mechanism. Photoionization and charge exchange are now generally regarded as the most effective mechanisms leading to ionization. Table I (Arpigny, 1965) lists the lifetimes for the two processes and the cross section for the case of charge exchange.

TABLE I

Molecule	CO	N	CN
τ (chg. exch.)	1×10^6	1×10^7	1×10^7
τ (photoion.)	0.5×10^7	0.3×10^7	10^7
σ_e (cm^2)	3×10^{-15}	1×10^{-15}	1×10^{-15}

Marochnik (1963) has suggested another mechanism which may play a role in ionizing cometary neutrals. He assumes that those molecules ionized by photoionization and charge exchange load the solar flow so that considerably more massive particles are available to bombard the neutrals. Possible collisional reactions include:



The advantage of this mechanism is that a given initial ion produces two second generation ions which (after they have become frozen into the solar wind) are then available to produce yet two more

ions. The process has been aptly termed "cascade ionization". Marochnik estimates the lifetime for ionization of N_2 and CO by this process to be about $10^{3.5}$ seconds.

Several authors have pointed out the likelihood of the formation of a shock front on the sunward side of a comet (Alfven, 1957; Marochnik, 1963; Axford, 1964). Axford postulates that if such a shock exists, heating across it may be sufficient to provide ionization by electron collisions. He speculates that electron thermal energies of the order of 1-10 KeV may result. At these energies, the cross section for collisional ionization is about 10^{-16} cm² (only an order of magnitude less than the cross section for ionization by charge exchange). Even if only a relatively small number of electrons reach these energies, this mechanism can be effective since a given electron can produce many ions whereas, in the charge exchange process, a given proton can produce only one ion.

Hubner (1961), following Fahleson (1961) and Alfven (1961), has suggested yet another ionization mechanism. As the solar plasma collides with the comet's coma, neutral comet molecules will knock out solar wind protons leaving localized pockets of charge imbalance. In the presence of the solar wind's frozen-in magnetic field, the electrons cannot immediately neutralize this imbalance. The potential tending to remove electrons from the region will cause an increase in their velocity around and along field lines. The local electron temperature may thus rise to a level where the electrons become effective in ionizing neutrals.

Wurm (1963) maintains that all of these mechanisms lead to

inconsistencies. He favors a mechanism inherent to the comet itself and not involving the solar wind or solar radiation. However, he does not speculate or define what this mechanism might be.

D. The Tail

Whatever the ionization mechanism may be, its cumulative effect is the generation of a plasma tail (generally referred to as a type I tail). These tails point almost directly away from the sun and reach lengths of 10^6 - 10^8 kilometers. Characteristic of these tails are density fluctuations in the composite plasma. Such terms as clouds, condensations, streamers, and rays have been used to describe these various irregularities. Some of the density fluctuations, especially those of a highly erratic nature, are due to outbursts that first appear in the coma and subsequently move into the tail. Other variations appear to be intrinsic to the tail. Some of these latter variations show quite interesting features. For example, Wurm (1963) notes that the rays tend to occur in pairs symmetrical to the radius vector connecting the comet and the sun and that they rotate inward with a decreasing angular velocity.

The ions in localized regions of type I tails often have accelerations 100 times greater than the value of solar gravitational acceleration. It should be noted that radiation pressure is entirely inadequate to account for these observed accelerations - it is too small by two orders of magnitude. Biermann (1953) attributed the high accelerations to collisions between the incoming solar wind electrons and the cometary ions. He showed that a stream of particles of number density 10^3 cm^{-3} could account for the observed accelerations.

This figure is now known to be about two orders of magnitude higher than the actual solar wind density. Charge exchange with simultaneous momentum transfer has also been investigated and found to be inadequate to account for the acceleration of tail particles (Biermann and Trefftz, 1960).

Harwit and Hoyle (1962) invoked the so-called two stream instability as a possible means of explaining this phenomenon. In this process, translational kinetic energy carried by the in-coming solar wind electrons is transferred into an exponentially growing wave mode involving the cometary ions. The onset of this type of instability depends critically upon the electron temperature. Harwit and Hoyle conclude that instability may occur for brief periods, but that (in order to conserve energy) as momentum is transferred from solar wind electrons to the comet ions, the electron temperature becomes so high that stability is restored.

CHAPTER III

THE PROPOSED MODEL

A. Introduction

Much of the most recent work in the area of cometary physics has been aimed at analytically solving the problem of the solar wind flow past a comet (Ioffe, 1966; Kovar and Kern, 1966; Biermann, Brosowski, and Schmidt, 1967). The general approach is that of gas dynamics. The continuity of the solar wind flow is effected by its frozen in magnetic field. As has been previously noted, the fact that the solar wind moves at supersonic velocity has led many authors to postulate the formation of a shock upstream from the comet (Alfven, 1957; Marochnik, 1963; Axford, 1964; Ioffe, 1966). A particular difficulty in solving the flow problem is the modification of the hydrodynamic equations to include source terms. Molecules sublimated from the nucleus become ionized and eventually load the solar flow. Still another difficulty is that the plasmas considered are compressible.

B. Discussion of the Proposed Model

A distinguishing feature of the comet-solar wind interaction is the formation of a contact discontinuity which separates purely cometary material from solar wind material. This surface acts like a blunt object in that the solar wind is forced to flow around it. The flow, then, is somewhat analogous to that of the solar wind past the earth, for here also a shock front and a contact discontinuity result. Figure 2 shows the orientation of the shock front and the

contact discontinuity relative to the comet's nucleus.

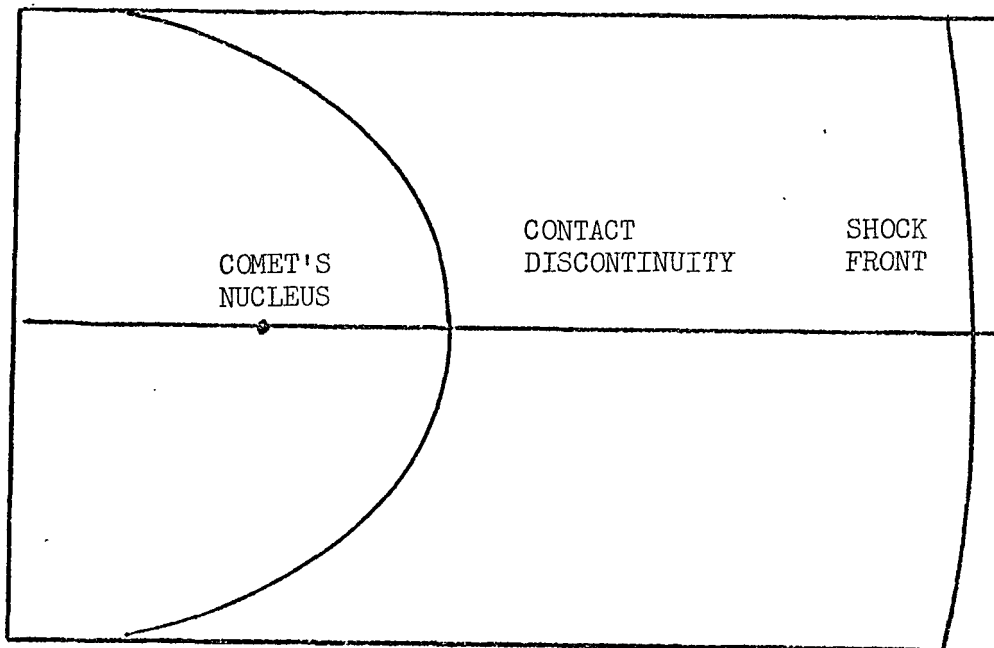


Figure 2

The purpose of the model investigated here is to find the size and shape of this contact discontinuity and the density of plasma interior to it. Several assumptions are made in the process of developing the model. Two are of sufficient importance to warrant detailed discussion, namely, that there is no magnetic field inside the contact discontinuity and that ions flowing from the nucleus are specularly reflected from this surface.

In previous treatments, the plasma flowing away from the comet's nucleus has been regarded as a continuous medium. Since the mean free path for collision of ions is very long ($\sim 10^5$ km), this assumption is questionable. To support this approach, the argument has been made that magnetic fields present in the comet's coma would provide continuity in the flow. However, it is to be

noted that, since the outflowing plasma is diamagnetic, it is highly probable that the region interior to the contact discontinuity will be devoid of a magnetic field.

If one accepts the existence of a contact discontinuity and also that the solar wind's magnetic field is frozen in, then obviously no magnetic field can penetrate the cavity since the field will be carried by as the solar wind flows past. However, several authors (Alfven, 1957; Marochnik, 1963) have speculated that the magnetic field carried by the solar wind may become partially trapped in the cometary plasma between the shock and the contact discontinuity. The problem then is to find the length of time it will take this field to diffuse into the plasma inside the cavity. A problem closely related to this one has been considered by Piddington (1959). He has calculated the time required for the earth's magnetic field to relax (through outward diffusion) after being compressed by the solar wind; he finds a relaxation time of about 18 years. The problem to be treated here is the inverse of the one considered by Piddington, i. e., in this case the magnetic field is diffusing from the solar wind rather than into it. An approximate value for the time, τ , required for the solar wind's field to diffuse into the cavity is given by $\tau = \pi \sigma R_0$, where R_0 is the radius of the cavity and σ is the conductivity of the plasma inside the cavity. Setting $\sigma = 10^{-14} T^{3/2}$, and with $T = 600^\circ$ K and $R_0 = 10^9$ cm, a value of $\tau = 10$ years is obtained.

With no magnetic field present, it can be assumed that the outflowing ions move independently of one another. When the ions

reach the boundry, the pressure they exert is just sufficient to balance the pressure of the solar wind. Exterior to the boundary, where magnetic fields are present, a continuous flow will exist. Assuming the solar wind's frozen in field to have a direction perpendicular to its flow direction, the magnetic field configuration will be one of concentric circles around the contact discontinuity. The outflowing ions will be deflected by this field back into the cavity. Assuming that energy and momentum are conserved, the ions will be specularly reflected from this boundary, i. e., their angle of incidence and reflection, with respect to a unit normal to the surface, will be equal.

Using these two assumptions, the size and shape of the contact discontinuity and the ion density interior to it will be determined. The contact discontinuity is treated in the following chapter and the ion density in Chapter V. The solution of both problems depends upon the density of outflowing ions. Thus, calculation of this density is now considered.

Inside the contact discontinuity only photoionization can be effective in converting the outflowing neutrals into ions. This simplifies the problem considerably. The nucleus is here treated as an isotropic point source of neutral molecules and the assumption is made that as the neutrals are ionized their velocity is unchanged. Thus, the net outflow of material, i. e., neutrals plus ions is governed by the equation $\nabla \cdot (\rho^* \bar{v}) = S\delta(\bar{r})$, where ρ^* is the total density - neutrals plus ions, \bar{v} the average ejection velocity of neutrals from the comet's nucleus, and S the mass production rate. This equation can

be integrated to give

$$\rho^* = (S/4\pi v) (1/r^2). \quad (1)$$

Let ρ_n be the density of neutrals and ρ_o the density of ions. Then

$$\rho^* = \rho_o + \rho_n. \quad (2)$$

Since the neutrals are being ionized with time constant τ , the density of neutrals is determined by $\nabla \cdot (\rho_n \bar{v}) = -\rho_n/\tau$. Integration of this equation gives

$$\rho_n = (S/4\pi v) \exp(-r/v\tau)/r^2. \quad (3)$$

Equations (1), (2), and (3) then give for the density of ions:

$$\rho_o = (S/4\pi v) [1 - \exp(-r/v\tau)]/r^2. \quad (4)$$

CHAPTER IV
THE CONTACT DISCONTINUITY

A. The Pressure Equation

An analytic expression for the contact discontinuity can be obtained by balancing solar wind pressure and the pressure exerted by the outflowing ions. On the surface where the pressures balance

$$\rho_s v_s^2 (\bar{v}_s / v_s \cdot \bar{n})^2 = \rho_0 v^2 (\bar{v} / v \cdot \bar{n})^2 \quad (5)$$

The s subscripts refer to the solar wind and \bar{n} is a unit normal pointing in the outward direction. The geometry involved is shown in Figure 3. In this figure, the variables R, ϕ are used to locate points on the surface.

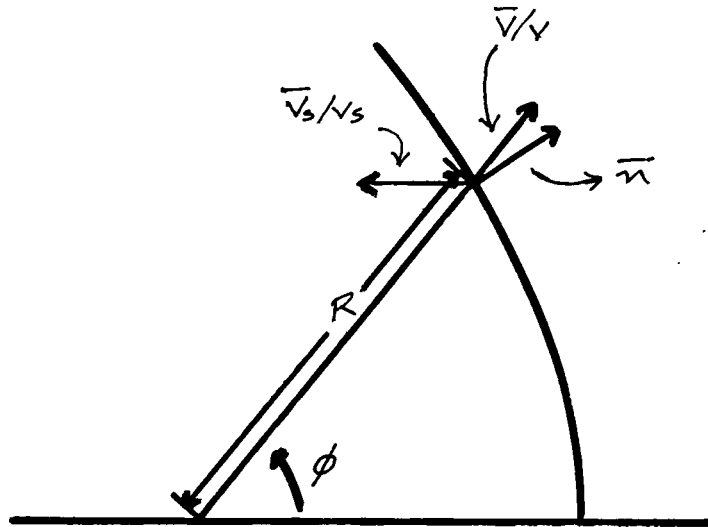


Figure 3

Let \bar{e}_r and \bar{e}_θ denote unit vectors parallel and perpendicular to the radial direction. Then the following relationships hold:

$$\begin{aligned}\bar{v}_s/v_s &= -\cos\varnothing \bar{e}_r + \sin\varnothing \bar{e}_\theta \\ \bar{v}/v &= \bar{e}_r \\ \bar{n} &= \left[\bar{e}_r - 1/R \, dR/d\varnothing \bar{e}_\theta \right] / \sqrt{1 + (1/R \, dR/d\varnothing)^2}.\end{aligned}$$

Substituting these into equation (5) gives:

$$\sin\varnothing \, dR/d\varnothing + R\cos\varnothing = \sqrt{Sv/[4\pi\beta_s v_s^2]} \sqrt{1 - \exp(-R/v\tau)} \quad (6)$$

where β_s has been expanded according to (4). Note that as $\varnothing \rightarrow 0$, equation (6) gives an expression for R_0 , the on-axis distance where the pressures balance, i. e.,

$$R_0 = \sqrt{Sv/[4\pi\beta_s v_s^2]} \sqrt{1 - \exp(-R_0/v\tau)}. \quad (7)$$

Hence, equation (6) can be written

$$\sin\varnothing \, dR/d\varnothing + R\cos\varnothing = \sqrt{1 - \exp(-\beta R)} / \sqrt{1 - \exp(-\beta)}. \quad (8)$$

This is the basic equation determining the form of the contact discontinuity. R_0 has been set equal to unity with the understanding that it is the unit for measuring distance. The parameter β is defined by $\beta = R_0/v\tau$.

B. Calculated Shape of the Cavity

Unfortunately, equation (8) is non-linear and appears to have no solution in terms of familiar functions. However, for the special cases of $\beta \ll 1$ and $\beta \gg 1$, equation (8) reduces to, respectively,

$$\sin\varnothing \, dR/d\varnothing + R\cos\varnothing = \sqrt{R}$$

and

$$\sin\phi \, dR/d\phi + R\cos\phi = 1.$$

Both of these equations are soluble in terms of familiar functions.

The solutions, in order, are

$$R = 2F^2(Q)/\sin\phi$$

and

$$R = \phi/\sin\phi$$

where F is Legendre's elliptic integral of the first kind having modulus $\sqrt{2}/2$ and Q is given by: $Q = \cos^{-1}\sqrt{\tan[(\pi-\phi)/4]}$ (Byrd and Friedman, p. 710).

For the general case, where approximations to the exponential term in equation (8) cannot be made, numerical methods must be employed. In rectangular co-ordinates the equation to be solved is

$$dy/dx = y \left\{ x - (x^2 + y^2) \sqrt{[1 - \exp(-\beta)] / [1 - \exp(-\beta\sqrt{x^2 + y^2})]} \right\}.$$

In the range $0.01 < \beta < 1$, the two limiting cases fail. Values of β in this range were thus chosen and this equation was integrated using the Runge-Kutta method.

Figure 4 shows plots of the contact discontinuities for the two limiting cases. These curves represent boundaries within which curves in the intermediate of β ($0 < \beta < \infty$) must lie. If R is regarded as a function of both ϕ and β , i. e., $R=R(\phi, \beta)$, then as β varies from 0 to ∞ , all possible contact discontinuities are generated;

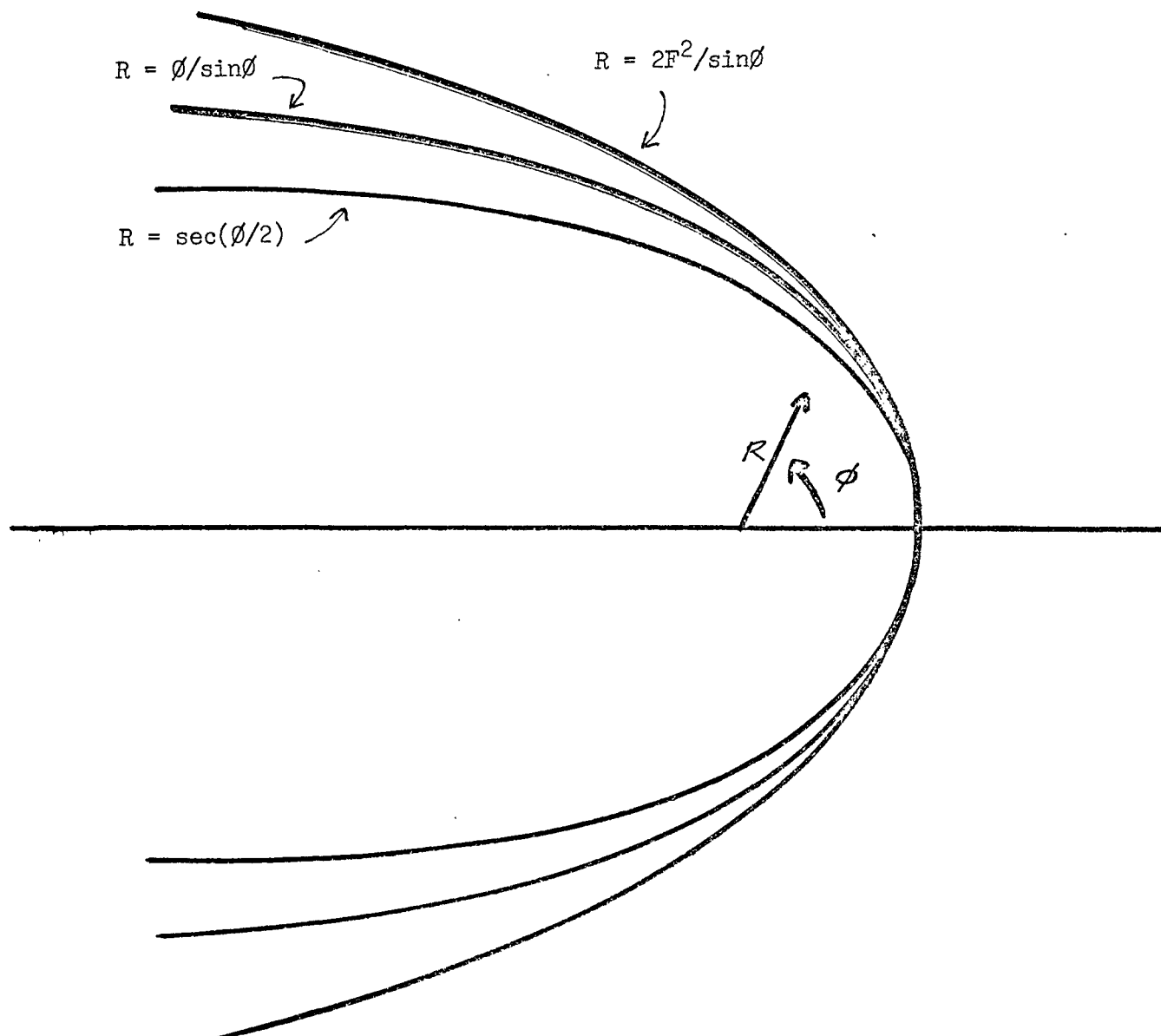


Figure 4

effectively, the outer boundary is rotated into the inner one. As can be seen from Figure 4, the shape of the contact discontinuity is relatively insensitive to the value of β . In this figure, for comparison purposes, a plot of the surface $R = \sec(\theta/2)$ is included. This contour is the continuation of the on-axis streamline (for the case of potential flow) of a uniform flux from infinity past an isotropic point source. The results of the numerical integration are shown in Figure 5. The upper and lower curves in this graph were calculated using the limiting cases. Again, the striking similarity in form of the surfaces is apparent.

C. Calculated Size of the Cavity

The size of the cavity can be determined as follows. Equation (7) for the on-axis stopping distance of the solar wind can be written $\beta^2 = \gamma [1 - \exp(-\beta)]$, where $\gamma = Nm_n [4\pi \rho_s v_s^2 v \tau^2]$. Here $S = Nm_n$, where N is the number of neutrals of mass m_n produced per second. If γ is specified, then β is determined. Once β is fixed, the cross section of the cavity at ∞ , R_∞ , is determined. Thus, the parameter γ determines the scaling of the cavity. In Figure 6 a plot of $\beta = \beta(\gamma)$ is shown. Now $R_0 = v\tau\beta$ and $N = [4\pi \rho_s v_s^2 v \tau^2 \gamma] / m_n$; hence, by adjusting the β - γ scales, this curve also represents $R_0 = R_0(N)$, i. e., the stopping distance as a function of the number of neutrals produced per second. To determine the scale factors, values must be assigned to the constants involved. The more abundant neutral molecules include CN, C₂, CO, and N₂. These all have molecular masses of $\sim 30m_p$, where m_p is the mass of a proton. The time constant is a more uncertain quantity. Its value will depend on the molecular

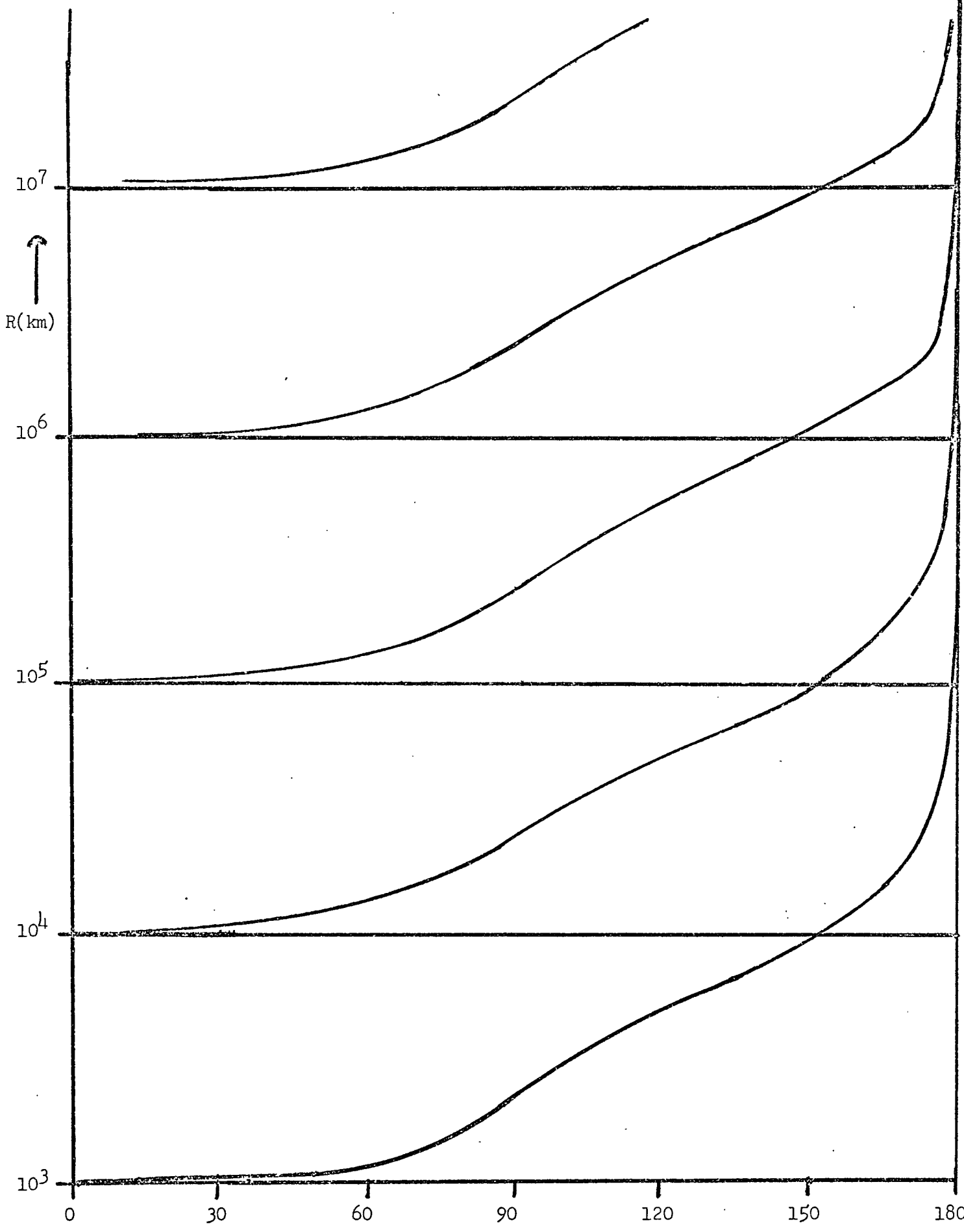


Figure 5

ϕ \rightarrow

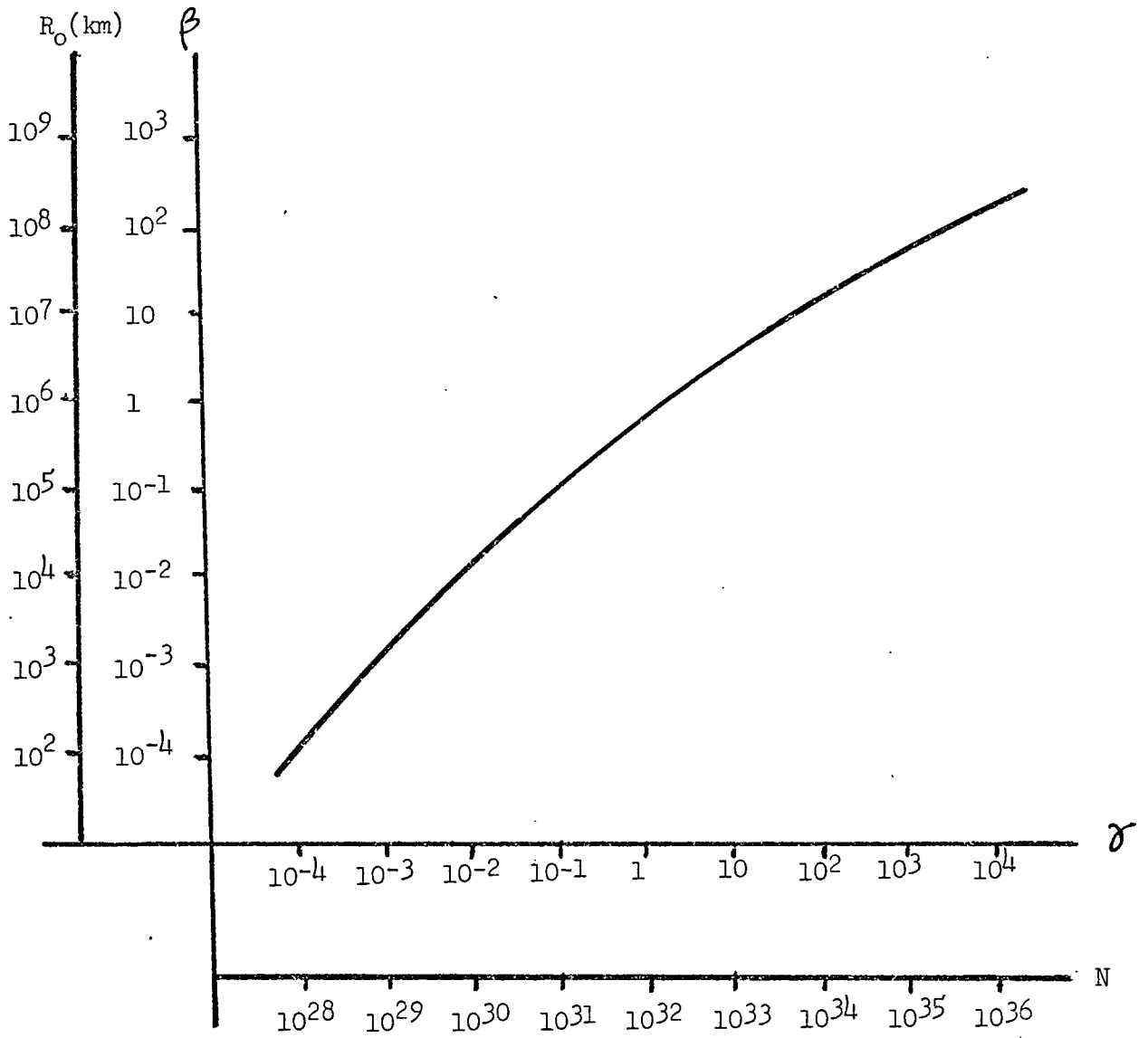


Figure 6

type. Thus τ should be regarded as an average. $\tau=10^6$ sec is adopted from Table I (Chapter II). Note that the scaling is fairly sensitive to the value of τ . For example, if $\tau=10^5$ sec, the numbers on the scale for N in Figure 4 would be reduced by a factor of 100 with corresponding R_0 values reduced by a factor of 10. The ejection velocity $v=10^5$ cm/sec has been adopted (Wurm, 1963). Values of β and v_s are those corresponding to a distance of 1 a. u. Table II lists these various parameters along with their values.

TABLE II

Parameter	m_n	v	τ	β_s	v_s
Value	$30 m_p$	10^5 cm/sec	10^6 sec	m_p/cm^3	4×10^7 cm/sec

With these values, then, $R_0=10^6 \beta$ and $N=10^{32} \gamma$, where R_0 is measured in kilometers. Figure 7 shows a plot of $R_0=R_0(N)$ in the range of most rapid change.

For the limiting case $\beta \gg 1$ the cross section of the cavity at ∞, R_π , is given by $R_\pi = \pi R_0$, while if $\beta \ll 1$, $R = 2K^2 R_0 \approx 6.68 R_0$, where K is Legendre's complete elliptic integral of the first kind with modulus $\sqrt{2}/2$. Figure 8 shows a plot of the ratio $R_\pi/R_0 = R_\pi/R_0(N)$. Values in the intermediate range of β were obtained by numerical integration. Note that the ratio effectively doubles from one limiting case to the next. This is to be expected since in the case where $\beta \gg 1$ the ion density falls off as $1/r^2$ whereas in the other limiting case, $\beta \ll 1$, the fall off is weaker, i. e., $\rho \propto 1/r$.

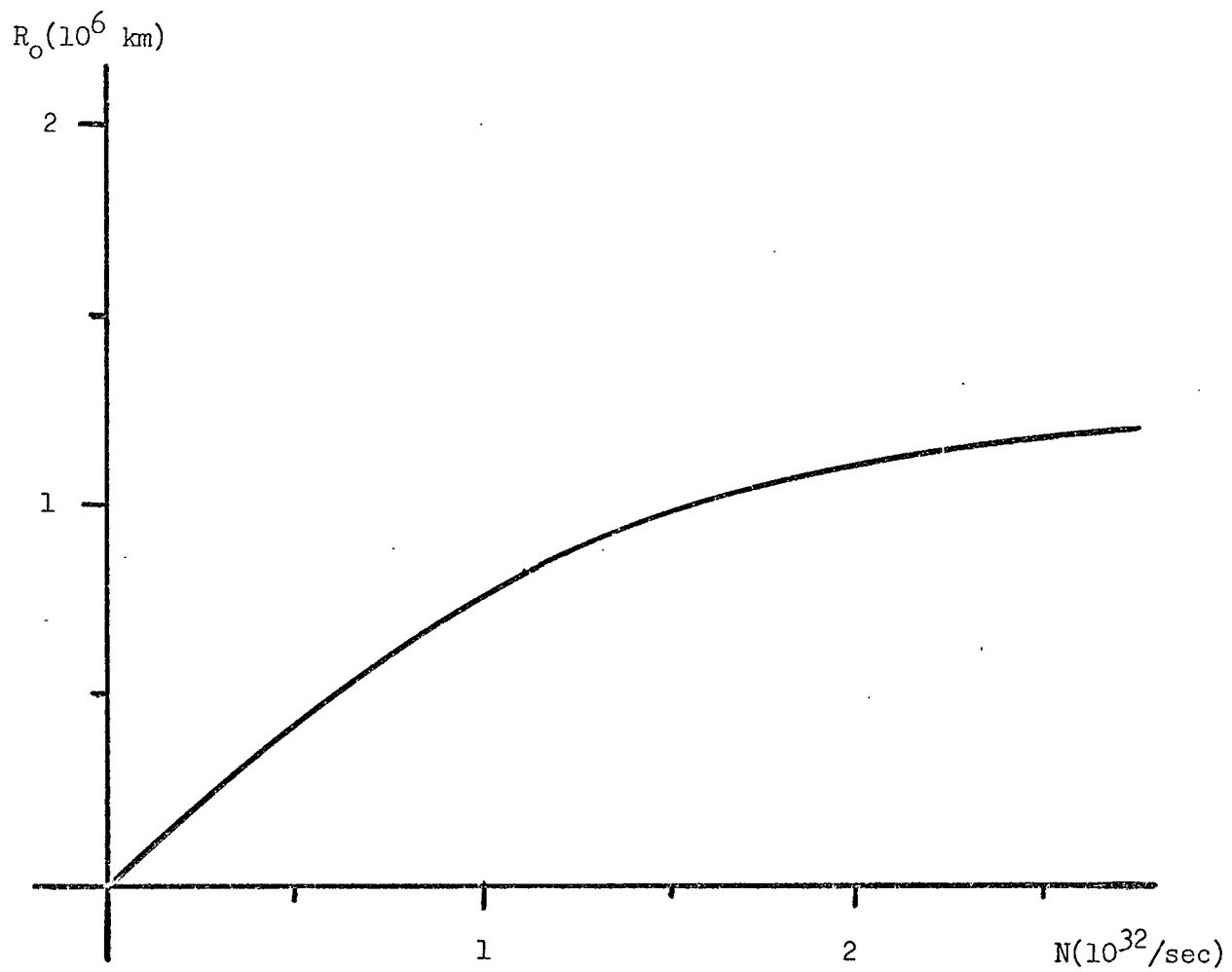


Figure 7

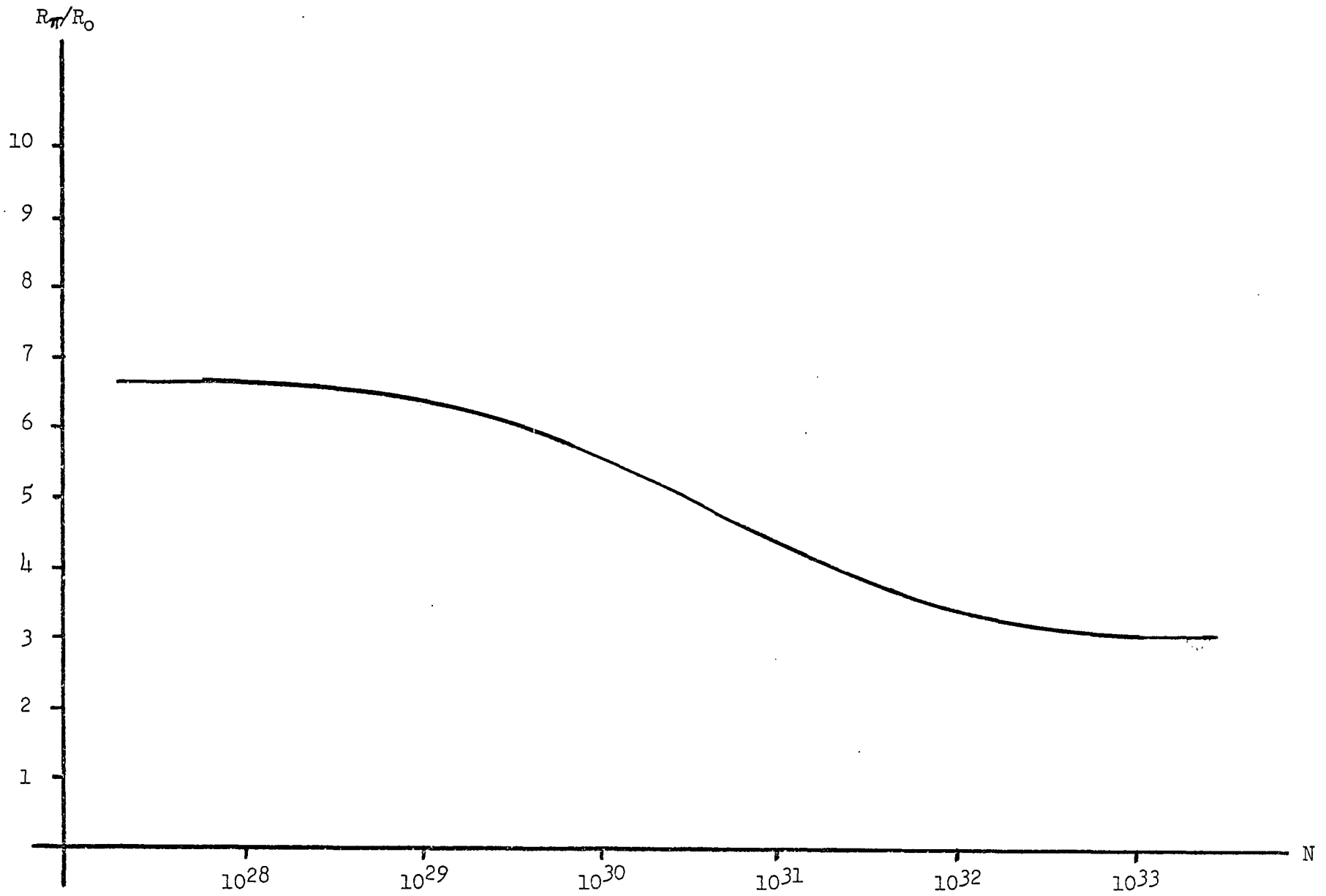


Figure 8

CHAPTER V

THE ION DENSITY IN THE COMA AND TAIL

A. The General Problem

The problem of finding the density of ions inside the cavity is now considered. At present, only part of the density is known, viz., the density due to ionization of the outflowing neutrals. However, in the discussion in Chapter III, the assumption was made that the outflowing ions were specularly reflected from the interior of the cavity. Hence, to find the total density, the contribution from not only the outflowing ions but also the reflected ions must be considered. Note that, formally, the reflection process can continue indefinitely. For the moment, only the density contribution from ions which have been once reflected will be considered. The problem of higher order reflections will be treated in Section E.

B. The Density Contribution from First Order Reflections

The density of ions due to first reflections can be found as follows. Consider that portion of the contour reached by ions flowing directly from the nucleus (but not by ions which have been once reflected) as an ion source. Let ions be emitted in a direction such that the inner normal to the surface of the cavity bisects unit vectors pointing toward the nucleus and along the emission direction. Let the intensity of the source be

$$\rho_0(R) = S/4\pi v [1 - \exp(-R/v\tau)] / R^2 .$$

By superposing the density due to this "line source" and the density

due to ions flowing directly from the nucleus, the net density is obtained.

The geometry involved in the reflection process is shown in Figure 9. The angle between the unit vector pointing toward the nucleus and the unit vector, \bar{e} , pointing along the emission direction is designated by ψ . The variables r, θ locate points inside the cavity.

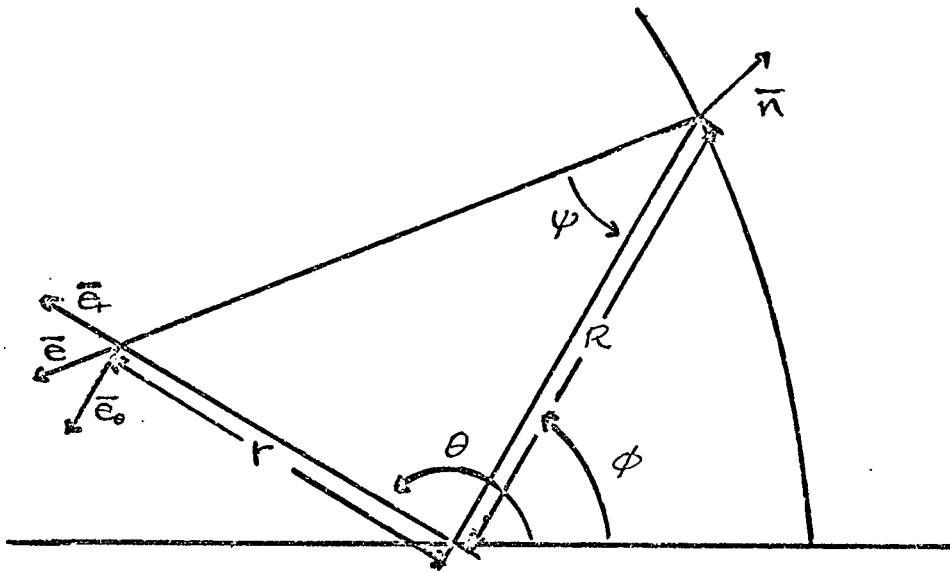


Figure 9

The ion flux, $\rho_i \bar{v}$, from the line source must satisfy $\nabla \cdot (\rho_i \bar{v}) = 0$, subject to the boundary condition that $\rho_i(R) = \rho_o(R)$. Expanding the continuity equation gives

$$\bar{e} \cdot \nabla \rho_i + \rho_i \nabla \cdot \bar{e} = 0. \quad (9)$$

Let the variable s denote distance along an ion trajectory measured from the surface. The solution of equation (9) is then

$$\rho_i = \rho_o(R) \exp\left(-\int_0^s \nabla \cdot \bar{e} \, ds\right). \quad (10)$$

It is convenient to make a change of variables from s to θ . Now

$$ds = \sqrt{r^2 + (dr/d\theta)^2} \, d\theta. \quad (11)$$

Using the law of sines in conjunction with Figure 9 gives

$$r \sin(\theta - \phi + \psi) = R \sin \psi. \quad (12)$$

Equation (12) can be used to reduce equation (11) to

$$ds = r \csc(\theta - \phi + \psi) \, d\theta. \quad (13)$$

The unit vector \bar{e} may be written as

$$\bar{e} = (\bar{e} \cdot \bar{e}_r) \bar{e}_r + (\bar{e} \cdot \bar{e}_\theta) \bar{e}_\theta. \quad (14)$$

From Figure 9 it can be seen that

$$\bar{e} \cdot \bar{e}_r = -\cos(\theta - \phi + \psi) \text{ and } \bar{e} \cdot \bar{e}_\theta = \sin(\theta - \phi + \psi). \quad (15)$$

Taking the divergence of equation (14) and using (15) gives

$$\nabla \cdot \bar{e} = [1/r] [-\cos(\theta - \phi + \psi) + \cot \theta \sin(\theta - \phi + \psi)]. \quad (16)$$

Substituting equations (13) and (16) into equation (10) and integrating gives for the reflected ion density

$$\rho_i = \rho_o(R) \sin \phi \sin(\theta - \phi + \psi) / [\sin \psi \sin \theta]. \quad (17)$$

Using equation (12), equation (17) becomes

$$\rho_i = \rho_o(R) R \sin \phi / [r \sin \theta]. \quad (18)$$

C. The Total Density

Thus far, it has been assumed that reflected ions from only one surface point can reach a given point inside the cavity. However, in general, this condition need not hold. To include the possibility of reflected ions from more than one surface point reaching a given r, θ , the reflected density must be summed. The total density, ρ , is then given by

$$\rho = \rho_0(r) + \sum_{j=1}^m \rho_0(R_j) R_j \sin \theta_j / [r \sin \theta]$$

where R_j, θ_j is the j^{th} set of values such that reflected ions from this point on the surface can reach a given r, θ and m is the total number of pairs. Expanding the expression for ρ using (4) gives

$$\rho = 1/r^2 \left\{ [1 - \exp(-\beta r)] / [1 - \exp(-\beta)] \right\} + \sum 1/R_j \left\{ [1 - \exp(-\beta R_j)] / [1 - \exp(-\beta)] \right\} \sin \theta_j / r \sin \theta$$

where the unit of density is $\rho_0(R_0)$. For the limiting cases of interest here, $\beta \ll 1$ and $\beta \gg 1$, the general solution reduces to, respectively,

$$\rho = 1/r + \sum \sin \theta_j / r \sin \theta \quad (19)$$

and

$$\rho = 1/r^2 + \sum \sin \theta_j / r R_j \sin \theta \quad (20)$$

Recall that the θ_j 's must satisfy equation (12). Now, since $\psi = 2 \tan^{-1}(1/R \, dR/d\theta)$, once $R=R(\theta)$ is specified and a point r, θ chosen, this equation determines a unique set of θ 's from which the density can be determined.

D. The Caustics

It should be pointed out that the number of roots of equation (12), i. e., m , depends upon the particular r, θ chosen. Perhaps the clearest way of showing the qualitative behavior of m is graphically. Note that in general equation (12) cannot be inverted to give ϕ as a function of r and θ . However, for $\theta = \pi$, this equation reduces to

$$r_{cr} = R \sin \psi \sin(\phi - \psi)$$

where r_{cr} is the distance at which ions reflected from R, ϕ cross the axis. This equation is sufficient to determine the qualitative behavior of m . If values are now chosen for ϕ , a set of trajectories for the reflected ions is obtained. This set of trajectories for the surface $R = \sec(\phi/2)$ is shown in Figure 10. Inspection of this figure indicates that a boundary exists which separates regions where $m=1$ and $m=3$. On the boundary itself, the value of m is not immediately obvious.

The problem of finding an analytical solution for the boundary is analogous to the optical problem of finding the curve enveloping light rays emanating from a point source and reflected from a curved mirror. Hence, this boundary will be referred to as the caustic. Let σ be the distance from the surface along an ion path to the caustic and r, θ the r, θ co-ordinates of the point the trajectory and the caustic have in common. Using the notation of Figure 9, the distance σ is given by

$$1/\sigma + 1/R = 2|k|/\cos(\psi/2) \quad (21)$$

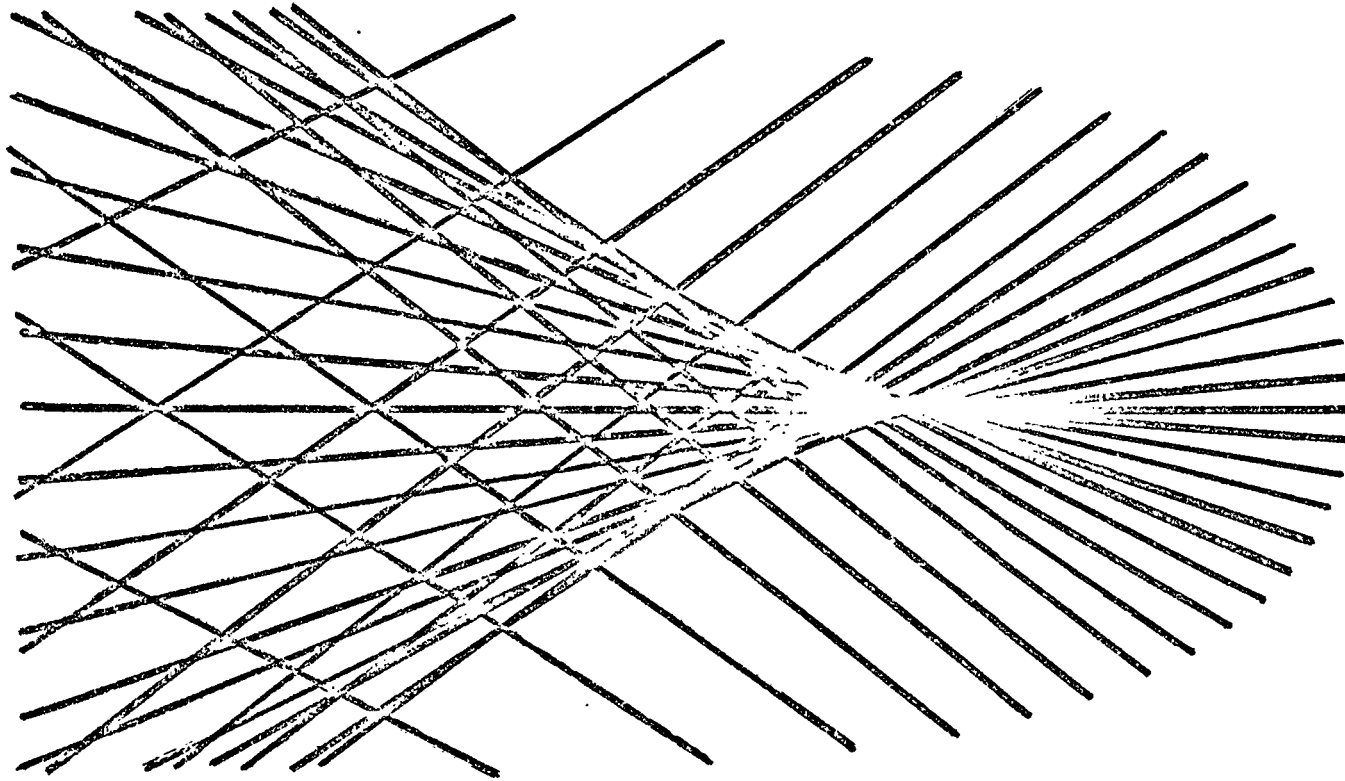


Figure 10

(Brand, p. 104). Here $k=k(\varnothing)$ is the curvature of the contact discontinuity which is given by

$$k = \left[R^2 + 2(dR/d\varnothing)^2 - R d^2R/d\varnothing^2 \right] / \left[R^2 + (dR/d\varnothing)^2 \right]^{3/2} .$$

For the surfaces considered here, $k > 0$, hence the absolute value sign is dropped in the following treatment. σ can be eliminated from equation (21) by using $\sigma/\sin(\chi - \varnothing) = R/\sin(\chi - \varnothing + \psi)$.

Equation (21) then becomes, after some reduction,

$$\chi = \tan^{-1} \left\{ \left[\sin(\varnothing - \psi) + G \sin \varnothing \right] / \left[\cos(\varnothing - \psi) + G \cos \varnothing \right] \right\} \quad (22)$$

where $G = 1 - 2kR/\cos(\psi/2)$, and from equation (12)

$$\Omega = R \sin \psi / \sin(\chi - \varnothing + \psi). \quad (23)$$

Equations (22) and (23) are thus parametric (parameter \varnothing) equations for the caustic. Equation (22) can be reduced to

$$\chi = \tan^{-1} \left\{ \left[H \sin \varnothing + I \cos \varnothing \right] / \left[H \sin \varnothing - I \cos \varnothing \right] \right\}$$

where $H = 2(1/R dR/d\varnothing)^2 - 1/R d^2R/d\varnothing^2$ and $I = 1/R dR/d\varnothing$. Thus χ is explicitly determined as a function of \varnothing once $R=R(\varnothing)$ is known.

Investigation of the caustics associated with the two limiting cases $\beta \ll 1$ and $\beta \gg 1$, reveals the same qualitative behavior as illustrated by Figure 10. In each case the caustic separates two regions in which reflected ions from either one or three surface points can contribute to the density. This results in a step function character for m , i. e., m has the value 1, 2, or 3 depending upon whether the point r, θ lies respectively interior to, on, or exterior

to the caustic. In Figure 11, plots of the caustics are shown. Two of these are cut off at the point of intersection with their associated contact discontinuities. The third caustic extends out to about $R=30$ before intersecting its associated contact discontinuity. Viewing from right to left, the caustics are associated with the surfaces $R=\sec(\theta/2)$, $R=\theta/\sin\theta$, and $R=2F^2/\sin\theta$.

It is essential to have an analytic form for the caustic in order to solve numerically for the contours of constant density. A computer program was employed to find the roots of equation (12) at about 300 $r-\theta$ lattice points interior to the cavity. On one side of the caustic, the program was devised to find only one root whereas on the other side three roots were found. Once the roots were found, the density was then calculated using equations (19) and (20). Contours were then found by linearly interpolating a certain value through the lattice of density values. Graphs and detailed discussion of these contours will be deferred to Chapter VI.

E. The Effects of Higher Order Reflections

A final problem remains, namely, consideration of the effects due to higher order reflections. The modifications involved are twofold. First of all, the shape of the contact discontinuity is modified. At the point where the caustic intersects the contact discontinuity as many as three contributions to the pressure may exist. Specifically, on the lower part of the surface, ions reflected from two upper surface points plus ions flowing directly from the nucleus are now available to exert pressure. One would expect the cavity to flare out due to the increased pressure. However,

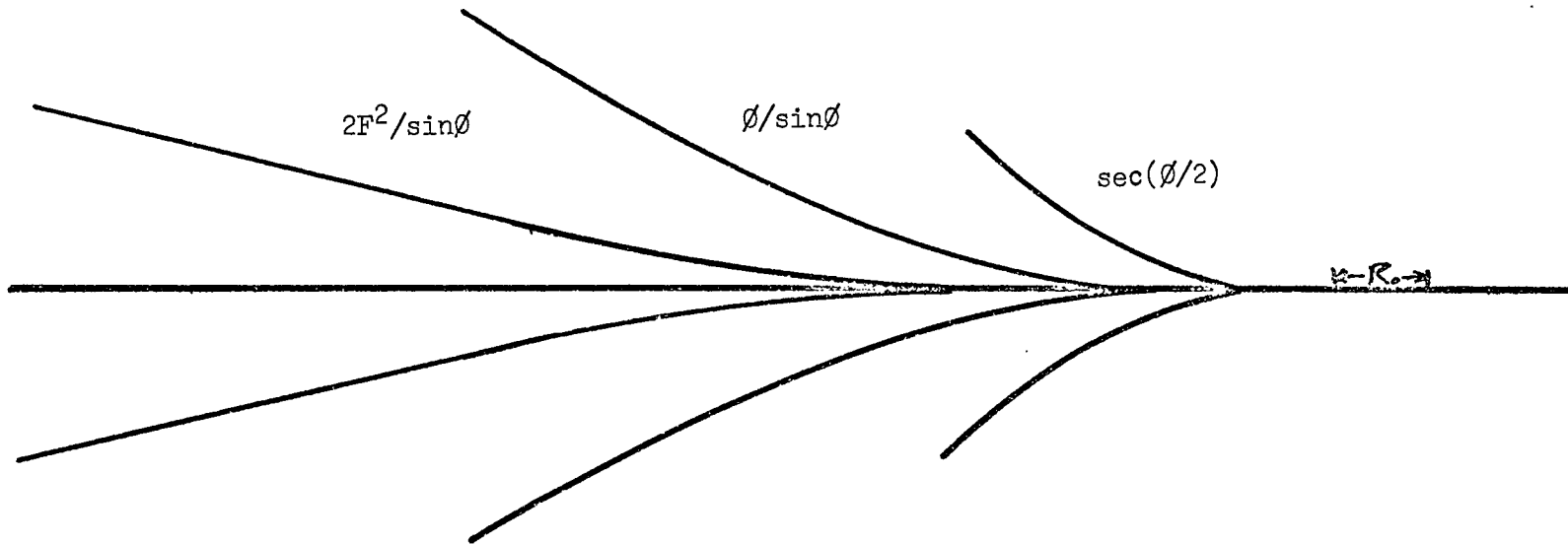


Figure 11

since pressure contributions fall off radially (direct ions) or as $1/y$ (reflected ions), where y is the distance from the axis, whereas the solar wind pressure has a constant value, eventually the boundary will tend toward a cylindrical form as was true of the original surface. The density inside the cavity is now found by superposing the density due to first and second order reflected ions and ions flowing directly from the nucleus.

Ideally the reflection process can continue indefinitely, in each case changing both the form of the contact discontinuity and the internal density. However, this will not occur for two reasons. First of all, it was initially assumed that the outflowing ions moved independently of one another since the mean free path for collisions was large. However, the reflection process leads to a focusing effect along the axis and the caustic so that the mean free path for collisions is drastically reduced. The result of collisions will be to reduce the directed mass flux available to exert pressure. Higher order reflections cannot be important for another reason. Even if collisions are completely neglected, the pressure contribution from higher order reflections is negligible compared to the pressure exerted by the ions flowing directly from the nucleus.

To support this statement, the equation which governs the shape of the new contact discontinuity if collisions are neglected is now investigated. This equation is

$$A_0 \rho_0 (\bar{v} \cdot \bar{n})^2 + \rho_1 (\bar{v}_1 \cdot \bar{n})^2 + \rho_2 (\bar{v}_2 \cdot \bar{n})^2 = \rho_s (\bar{v}_s \cdot \bar{n})^2.$$

The 1,2 subscripts refer to the two possible contributions due to reflected ions. The meaning of the constant A_0 will be explained presently. Expanding this equation gives

$$\begin{aligned} A_0/r^2 [1 - \exp(-\beta r)] - \sum \sin\phi_j / r R_j \sin\theta [1 - \exp(-\beta R_j)] D_j^2 \\ = [1 - \exp(-\beta)] (\cos\theta + \sin\theta/r dr/d\theta)^2 \end{aligned}$$

where D_j is defined by

$$D_j = \cos(\theta - \phi_j + \psi_j) + \sin(\theta - \phi_j + \psi_j)/r dr/d\theta$$

For the limiting case $\beta \ll 1$, the equation reduces to

$$\begin{aligned} A_0/r - \sum \sin\phi_j / r \sin\theta \left[\cos(\theta - \phi_j + \psi_j) + \sin(\theta - \phi_j + \psi_j)/r dr/d\theta \right]^2 \\ = (\cos\theta + \sin\theta/r dr/d\theta)^2 \end{aligned}$$

Rather than attempting to obtain a complete solution of the above equations, only the initial flaring of the cavity will be obtained. The initial point on the new contact discontinuity is determined by the intersection of the original caustic and contact discontinuity. For the particular surface $R = \sec(\phi/2)$, equation (22) can be inverted to give ϕ as a function of χ , i. e.,

$\phi = \tan(A + B)$, where

$$A = \left[\tan\chi/4 (1 + \sqrt{1 - 2\tan\chi}) \right]^{1/3}$$

and

$$B = \left[\tan\chi/4 (1 - \sqrt{1 - 2\tan\chi}) \right]^{1/3}.$$

The equation of the caustic can then be written explicitly as a function of χ ,

$$\Omega = R(\theta) \sin[\psi(\theta)] / \sin[\gamma - \theta + \psi(\theta)] \quad (24)$$

where $\psi(\theta) = 2 \tan^{-1} \left\{ \frac{1}{2} \tan(\theta/2) \right\}$. Let the point of intersection of the caustic and the contact discontinuity be at r', θ' . Thus θ' is determined as the root of

$$\sec[\theta(\theta')/2] \sin \{ \psi[\theta(\theta')] \} = -\sec(\theta'/2) \sin \{ \theta' - \theta(\theta') + \psi[\theta(\theta')] \}.$$

Solving gives $\theta' = 204^\circ \pm 0.1^\circ$ and $r' = 4.81$. With this initial point determined, it is possible to calculate all quantities in the pressure equation to determine $dr/d\theta$ at θ', r' and hence the flare angle f

$$f = \tan^{-1}(dy/dx) = \tan^{-1} \left\{ \frac{[\sin\theta' dr/d\theta + \cos\theta']}{[\cos\theta' dr/d\theta' - \sin\theta']} \right\}$$

where $dr/d\theta$ is evaluated at θ', r' .

In Figure 12 is shown a view of the region of interest.

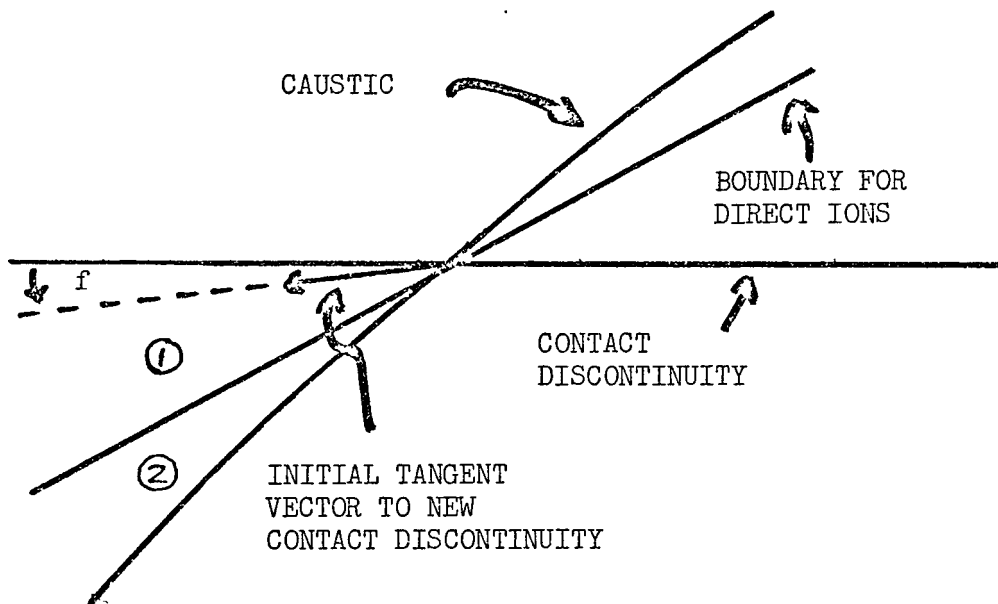


Figure 12

Since ion paths are tangent to the caustic and since direct ions cannot reach the region below the boundary indicated in Figure 12. (region ②), an upper limit on the initial direction of the cavity is determined. That is, the true direction of the vector tangent to the initial point of the new contact discontinuity must be rotated through some clockwise angle with respect to a vector tangent to the extension of the caustic. Two possibilities arise. If the vector tangent to the new surface lies in region ②, A_0 must be set = 0 (direct ions cannot reach this region to exert pressure); but if the vector lies in region ①, $A_0=1$. Calculation shows that on the boundary itself (where $dr/d\theta=\infty$), at the initial point, solar wind pressure is greater than internal pressure by a factor of 4 (for the case $\beta \ll 1$). Hence the tangent vector lies in region ① where $A_0=1$. Further calculation gives the flare angle as $f=7^\circ$. Since this angle is rather small, the radius of the cavity at infinity is not changed significantly from the value previously found. Actually, this angle should be regarded as an upper limit. The calculation was done assuming that the reflected ions were fully effective in exerting pressure. However, it has already been noted that collisions will tend to disperse the ion velocities and thus reduce the directed mass flux available to exert pressure.

The question arises as to the value of the angle f for the surfaces $R=r/\sin\theta$ and $R=2F^2/\sin\theta$. The similarity in form of the surfaces, caustics and contours of constant density suggests that the angle f will not change significantly for the other surfaces.

In any event, an actual calculation for these two cases would only give a limiting value since the reduction in effectiveness of the reflected ions in exerting pressure is not known.

CHAPTER VI

APPLICATION OF MODEL TO ACTUAL COMETS

A. Shape of the Contact Discontinuity

Empirical curve fitting has shown that the outline of the contact discontinuity, on the sunward side, can be approximated by either a parabola (Alfven, 1957) or a catenary (Marochnik, 1962). Now, the equation of the catenary, $x = 2a - a \cosh(y/a)$, can be expanded to give

$$x = a - \left[\frac{1}{(2!a)} \right] y^2 - \left[\frac{1}{(4!a^3)} \right] y^4 - \dots \quad (25)$$

which, to first order, reduces to a parabola. The catenary, then, probably gives a somewhat more accurate fit since it provides a second order correction. To compare the contour obtained here with these results, the general equation of the contact discontinuity in rectangular co-ordinates,

$$dx/dy = \left\{ x - (x^2 + y^2) \sqrt{\frac{1 - \exp(-\beta)}{1 - \exp(-\beta \sqrt{x^2 + y^2})}} \right\} / y,$$

is expanded. To second order the expansion gives

$$x = R_0 - \left[\frac{C_2}{(2!R_0)} \right] y^2 - \left[\frac{C_4}{(4!R_0^3)} \right] y^4 - \dots \quad (26)$$

where

$$C_2 = C_2(\beta) = (4 - \epsilon)/(6 - \epsilon)$$

$$C_4 = C_4(\beta) = \left[\frac{3(4 - \epsilon)^3 - 6\epsilon(6 - 2\beta - 3\epsilon)}{(10 - \epsilon)(6 - \epsilon)^3} \right]$$

$$\epsilon = \beta \exp(-\beta) / [1 - \exp(-\beta)]$$

Recall that β is a dimensionless parameter given by $\beta = R_0/v\tau$.

Note that to first order equation (26) also reduces to a parabola.

Let $a=R_0/C_2$ in equation (26). This equation then becomes

$$x = aC_2 - \left[1/(2!a)\right] y^2 - \left[\lambda/(4!a^3)\right] y^4 - \dots \quad (27)$$

where $\lambda=C_4/C_2^3$. As β varies from 0 to ∞ , λ varies from 1.3 to 1.8; hence, to second order, equation (27) closely approximates a catenary for all values of β . Figure 13 shows a parabola, catenary, and the contour obtained here for the case $\beta \gg 1$.

Note that all terms in equation (25) and (26) are of even order. Hence, to third order, equation (26) will still closely approximate the catenary. For large values of x , however, the catenary has an infinite width. Observationally, as pointed out by Ioffe (1966), at large distances from the nucleus the contact discontinuity approaches a cylindrical form. Hence, only in the head region will the catenary fit the true boundary. Equation (26) not only provides an accurate fit to the cavity outline on the sunward side but also defines a curve with a finite width at infinity.

B. The Contours of Constant Density

Figures 14 and 15 show the density contours associated with, respectively, very small and very large values of β (or, equivalently, very small and very large mass production rates). Figure 16 shows the contours which would result if the form of the boundary were given by $R=\sec(\theta/2)$. The unit of density, $\rho_0(R_0)$, can be found

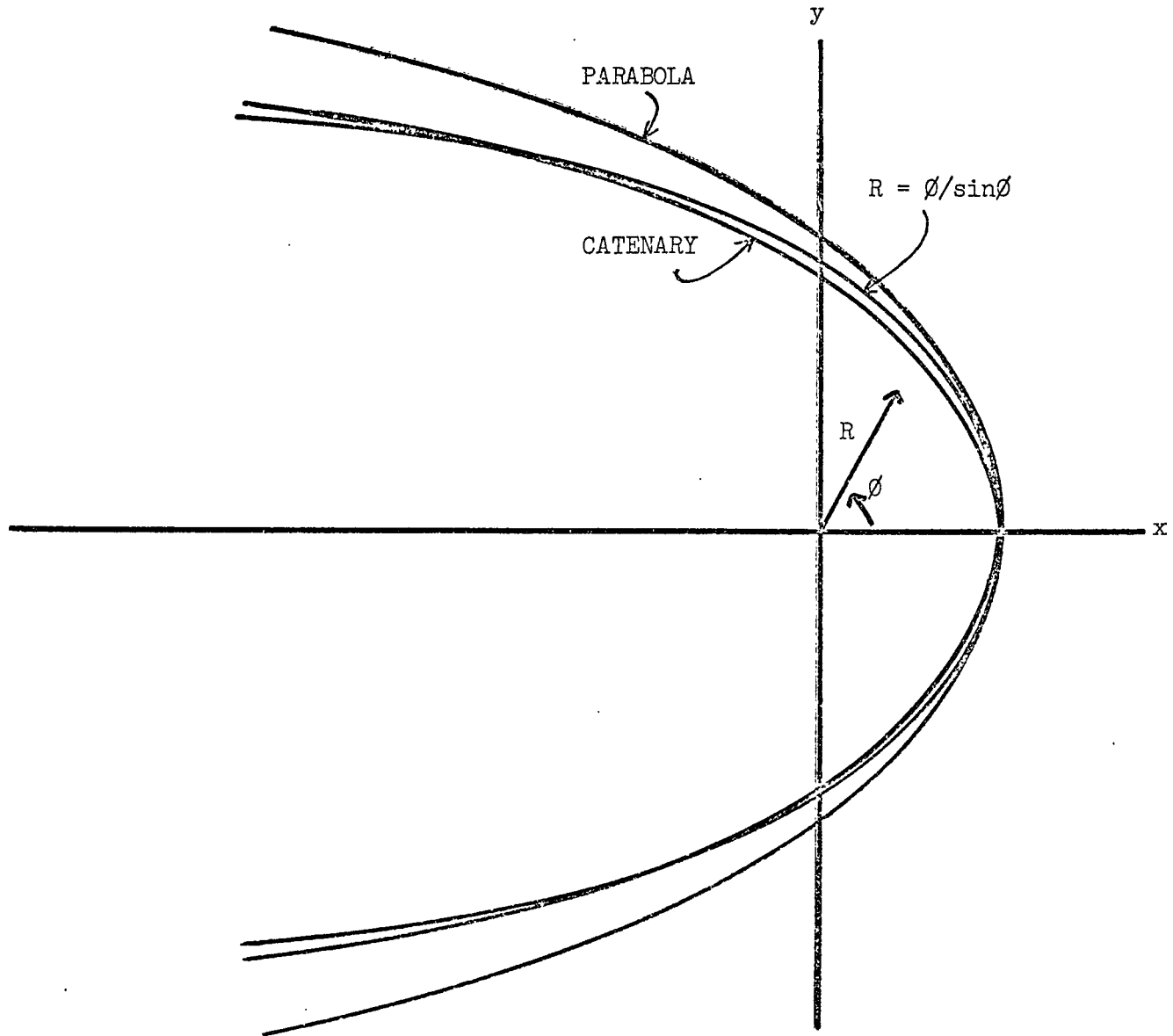


Figure 13

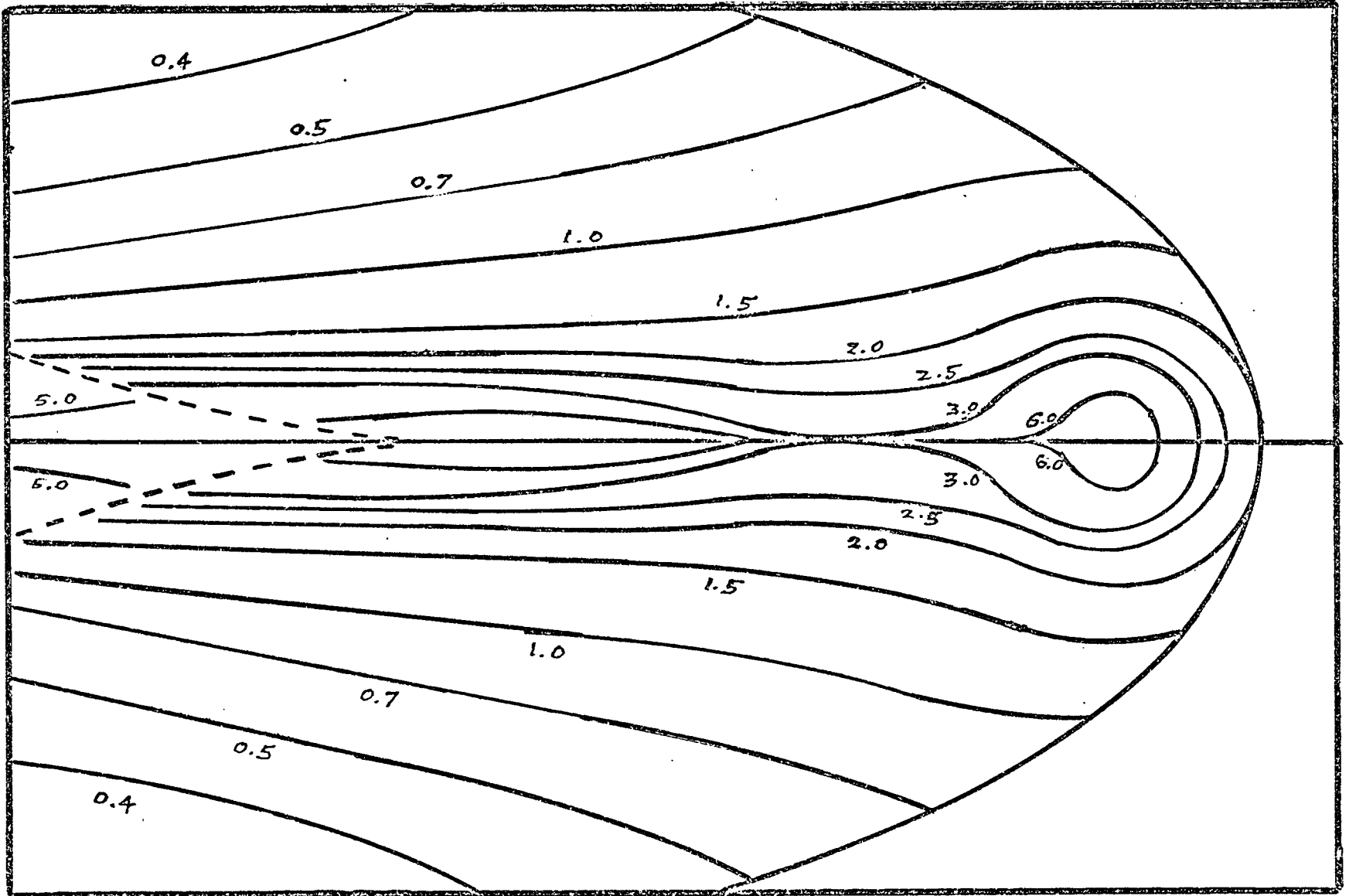


Figure 14

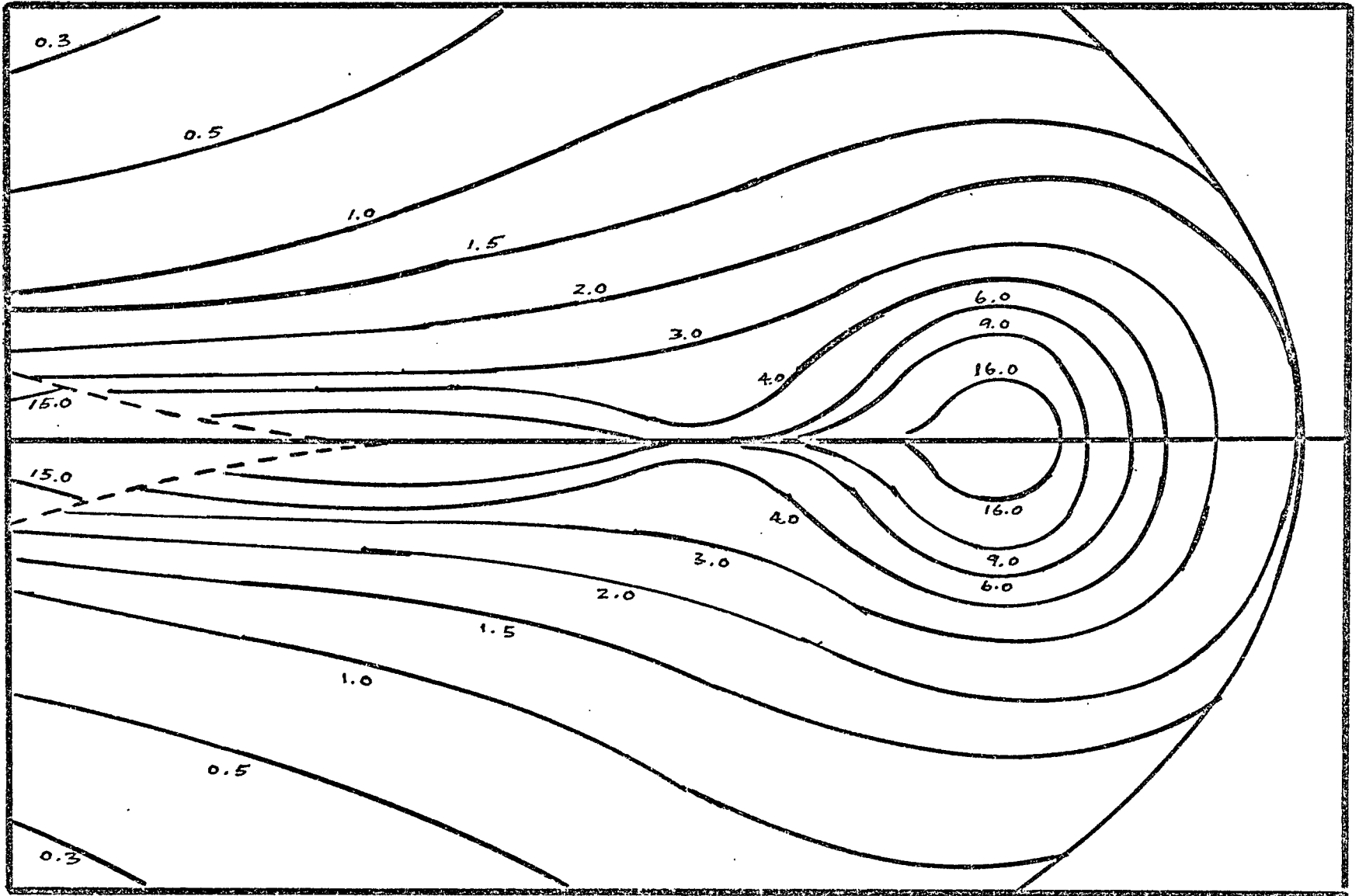


Figure 15

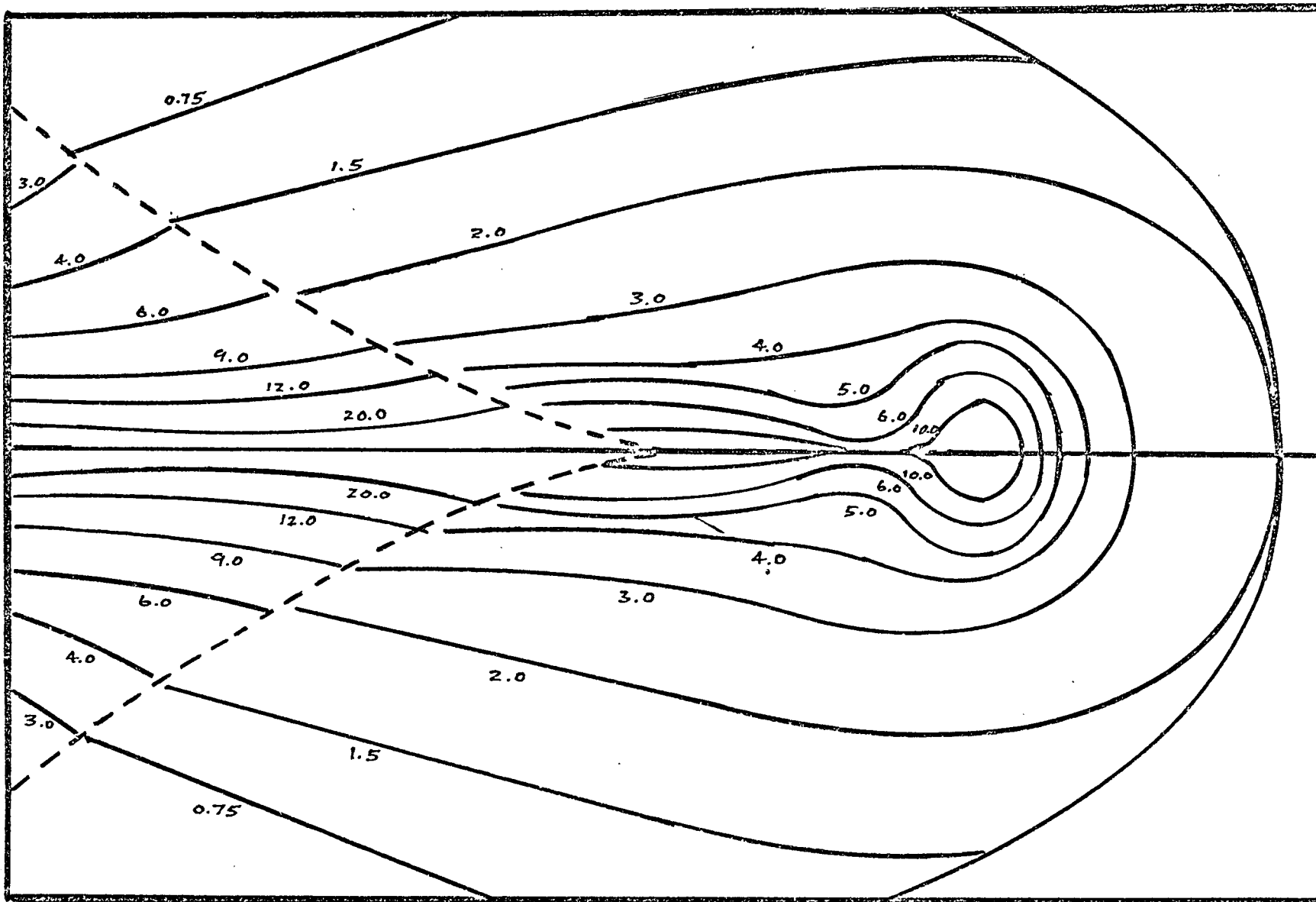


Figure 16

using equation (5) along with values for the physical parameters given in Table II. Thus $\rho_e(R_0) = 1500 \text{ m}_p/\text{cm}^3$ or about $500 \text{ ions}/\text{cm}^3$. Since the production rate and on-axis stopping distance change in such a way that equation (5) always holds, the unit is the same for all cases. It agrees reasonably well with the average value of $300 \text{ ions}/\text{cm}^3$ found by Wurm (1963) for the tail region of Halley's Comet.

It is apparent from inspection of the density contours that a general similarity exists among the various cases. In the head region the contours are roughly circular. As a contour is followed into the tail, a gradual straightening occurs. A discontinuity occurs across the caustic interior to which the contours again straighten as they are followed still further into the tail.

The most striking feature of the model is the prediction of the caustic surface (the dashed curves in Figures 14-16). For steady state conditions, the distance in units of R_0 from the nucleus where this surface intersects the axis is given by

$$R_c = 4/(2 - \epsilon).$$

Thus R_c decreases monotonically from 4 to 2 as β varies from 0 to ∞ . Moreover, as β varies through this same range, the distance from the nucleus (in units of R_0) to the point where the caustic intersects its associated contact discontinuity decreases from about 30 to 10. Since the density has a marked increase across this surface, it may correspond to an observable feature in a comet; the symmetry with

respect to the axis is highly suggestive of the rays.

C. Time Dependent Phenomena

The model to this point has been developed assuming steady state conditions. However, it is well known that the production rate of neutrals can vary. Outbursts (discussed in Chapter II) are generally regarded as being due to a sudden increase in the production rate of neutrals. Furthermore, as noted by Beard (1964), more uniform increases or decreases in the production rate may occur over extended periods of time. For example, if more or less stratified layers rich in dust and ice exist, the production rate will decrease as an icy layer, rich in volatile molecules, is depleted.

A sudden increase in the production rate would, according to the model developed here, result in the apparent motion of matter along the caustic. That is to say, the density along the caustic would not increase instantaneously at all points to a new level due to the different path lengths associated with the ion trajectories reaching this surface. Rather, the increase would first occur at the point closest to the nucleus and move outward. If the outburst were localized in a short time interval, there would be an actual motion of the increased density along the caustic giving the illusion that matter in a localized region was in motion. Clouds or condensations might be accountable for by this mechanism.

A final phenomenon the proposed model may explain is the rotation of the rays. As previously noted, the distance of the caustic from the axis depends upon the on-axis stopping distance which, in turn,

depends upon the production rate of neutrals. Thus, larger production rates correspond to closer distances to the axis. If, indeed, the caustic is a ray, an increase or decrease in production rate would result in inward or outward rotation respectively. Figure 17 shows the successive positions of the rays as the production rate increases by integral steps from some initial value.

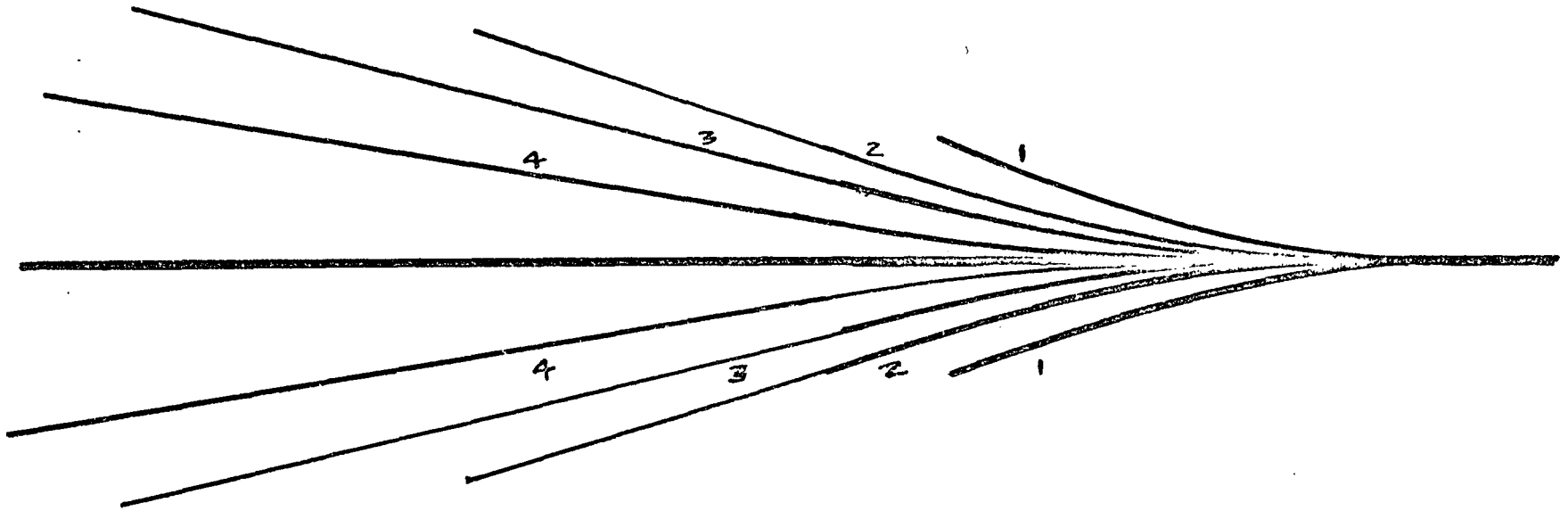


Figure 17

CHAPTER VII

SUMMARY AND CONCLUSIONS

The major assumptions of the present model are that ions move away from a comet's nucleus independently of one another and that they are specularly reflected from the interface separating cometary material from the solar wind. Utilizing these assumptions, a model was developed which predicted the size and shape of the contact discontinuity and the plasma density interior to it. In addition, the model predicted the existence of structure in a comet's tail. Previous models, which have treated the outflowing ions as a continuous medium, give solutions for the density which show no pronounced irregularities.

The present model is able to account for the observed outline of the contact discontinuity and for the finite width of the tail. The predicted mean ion density agrees well with Wurm's (1963) value based upon the intensity of radiation scattered from the tail ions. Plausibility arguments (Chapter VI) show that certain time dependent phenomena, in particular, the motion of clouds or condensations in the tail and the collapsing of the rays, may be explainable in terms of the model.

In summary, the conclusions reached are:

1. The observed outline of the cavity around a comet is closely approximated by the boundary obtained here.
2. The finite width of type I comet tails is explainable by the model.
3. The mean density of ions agrees with published data within observational error.

4. The existence of tail structure is predicted by the model and, again, this result agrees with observational data.
5. Certain time dependent phenomena, such as the rotation of rays and the motion of clouds or condensations, may be explainable in terms of the model.

REFERENCES

- Alfven, H. 1957, Tellus, 9, 92.
- _____ 1961, Rev. Mod. Phys., 32, 710.
- Arpigny, C. 1965, A Study of Physical and Molecular Processes in Comets (Mem. in 8 ac. R. Belg.).
- Axford, W. I. 1964, Planet. Space Sci., 12, 719.
- Beard, D. B. 1966, Planet. Space Sci., 14, 303.
- Beer, A., Lyttleton, R. A., and Richter, N. B. 1963, The Nature of Comets (London: Methuen and Co., Ltd.).
- Biermann, L. 1953, La Physique des Comets, (Report of 4th Liege Symposium).
- Biermann, L. and Treffitz, E. 1960, Zs. f. Ap., 49, 111.
- Biermann, L. and Lust, R. 1963, The Moon, Meteorites, and Comets, ed. Middlehurst, B. M. and Kuiper, G. P. (Chicago: The University of Chicago Press).
- Biermann, L., Brosowski, B. and Schmidt, H. U. 1967, Solar Physics, 1, 254.
- Brand, L. 1947, Vector and Tensor Analysis (New York: John Wiley and Sons, Inc.).
- Byrd, F. P. and Friedman, M. D. 1954, Handbook of Elliptic Integrals for Engineers and Physicists (New York: Lange, Maxwell, and Springer, Ltd.).

Cherenichenko, V. I. 1959, Soviet Astron., 3, 254.

Fahleson, U. V., 1961, Phys. Fluids, 4, 123.

Harwit, M. and Hoyle, F. 1962, Ap. J., 135, 875.

Hubner, W. 1961, Rev. Mod. Phys., 33, 498.

Ioffe, Z. M. 1966, Soviet Astron., 10, 138.

_____ 1966, Soviet Astron., 10, 517.

Kovar, N. S. and Kern, J. W. 1966, A. J., 71, 861.

Kovar, N. S. and Kovar, R. P. 1965, Ap. J., 142, 1191.

_____ 1966, A. J., 71, 166.

_____ to appear in Solar Physics April, 1968.

Marochnik, L. S. 1963, Soviet Astron., 6, 532.

Piddington, J. H. 1959, Geophys. Jour. Roy. Astron. Soc., 2, 173.

Preston, G. W. 1967, Ap. J., 147, 718.

Remy-Battiau, L. 1962, Ann. d'ap., 25, 171.

Swings, P. 1965, Roy. Astron. Soc., London, Quat. Jour., 6, 28.

Whipple, F. L. 1955, Ap. J., 111, 375.

_____ 1963, The Moon, Meteorites, and Comets, ed. Middlehurst, B. M. and Kuiper, G. P. (Chicago: The University of Chicago Press).

Wurm, K. 1963, The Moon, Meteorites, and Comets, ed.
Middlehurst, B. M. and Kuiper, G. P. (Chicago:
The University of Chicago Press).